Article

Construction of a Hollow Spherical Covalent Organic Framework with Olefin and Imine Dual Linkages Based on Orthogonal Reactions

Jingtao Hu, Junjie Zhang, Zhangxiang Lin, Lili Xie,* Saihu Liao, and Xiong Chen*

Cite This: https://doi.org/10.1021/acs.chemmater.2c00922

Read Online

ACCESS | Metrics & More | Article Recommendations | Supporting Information

ABSTRACT: Covalent organic frameworks (COFs) have widespread applications in many fields. However, successful attempts to construct COFs through the formation of two types of covalent bonds remain limited and challengeable. Here, we report the first example of a COF with olefin and imine dual linkages, which was enabled by orthogonal Schiff base reaction and the Knoevenagel condensation. The obtained COF-FD1 exhibits good stability and high selectivity in the fluorescence sensing of Fe^{3+} ions. Remarkably, this COF features a relatively rare hollow spherical morphology, and a time-dependent study of the continuous transformation from initial solid spherical to hollow spherical structures reveals an Ostwald ripening mechanism. This research not only demonstrates a new approach for the design and synthesis of COFs with dual linkages but also may bring about the possibility of constructing COFs with hollow structures.
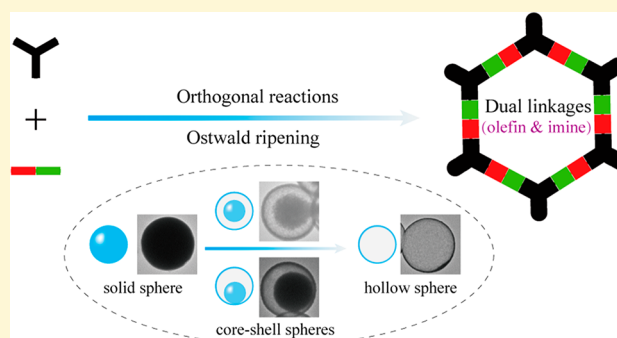
INTRODUCTION

Covalent organic frameworks (COFs) make up an emerging class of two-dimensional (2D) and three-dimensional (3D) crystalline porous polymers, with an exceptional diversity of types and shapes, due to the high accessibility and diversity of organic building blocks.[1−20] Meanwhile, these materials usually exhibit low densities, large specific surface areas, high thermal stabilities, and controllable structures, rendering them good candidates for various potential applications, including gas adsorption,[21−23] organic catalysis,[24−26] photocatalysis,[27−32] electrochemistry,[33−42] molecular recognition,[43] fluorescence sensing,[44−50] etc. COFs are constructed typically by interconnecting the molecular building blocks; therefore, the reversibility of the condensation reactions for the synthesis of highly crystalline COFs is particularly critical, while the formation of strong covalent bonds often leads to poor crystallinity or even an amorphous network. So far, a number of COFs have been successfully constructed through the formation of different covalent bond linkages, such as B−O, B−N, C=N, C−N, C=C,[51−54] etc., but a vast majority of COFs are connected by a single type of covalent bond. In contrast, only a few COFs are connected by more than one type of covalent bond,[55,56] though developing new synthetic strategies and constructing new COFs with dual linkages could greatly enrich the types, quantities, and functions of COFs. In particular, COFs with dual linkages could integrate the physical and chemical properties of two different connectors, affording dual-functional or specific functional materials without post-modification.[57,58,62]

The construction of COFs with dual linkages requires the formation of two types of covalent bonds; difficulty was often encountered in the compatibility of the two types of covalent bonds and/or the bond forming reactions. In 2015, Zhao et al. demonstrated the first successful synthesis of COFs with dual linkages using an orthogonal reaction strategy.[56] Since then, the construction of COFs by integrating two types of covalent bonds has attracted considerable research interest, and various novel COFs have been successfully synthesized with different dual linkages, including boroxine and hydrazone linkages,[57] boroxine and triazine linkages,[58] etc. However, so far, the most frequently reported examples were constructed by employing the B−O bond as one end of the connection core by virtue of its dynamic reversibility.[55−63] On the contrary, the unstable nature of the B−O bonds often restricted the stability and function of these dual-linkage COFs. Here, we report a new strategy for constructing COFs by combining Schiff base reaction and the Knoevenagel condensation, allowing the synthesis of a new type of COF for the first time with olefin and imine dual linkages, denoted as COF-FD1 (Scheme 1).

It is well-known that the Schiff base reaction is reversible,[64] while for the Knoevenagel condensation reaction, strong

Scheme 1. Strategy for Preparing COFs with Olefin and Imine Dual Linkages, Including (a) a Schematic Representation of the Bifunctional Linker 4-Aminobenzyl Cyanide Along with the Linkage Structure of the COF with Dual Linkages, (b) the Model Reaction of Benzaldehyde with 4-Aminobenzyl Cyanide to Form the Dual Linkages, and (c) Synthesis of COF-FD1 with Dual Linkages via Orthogonal Reactions
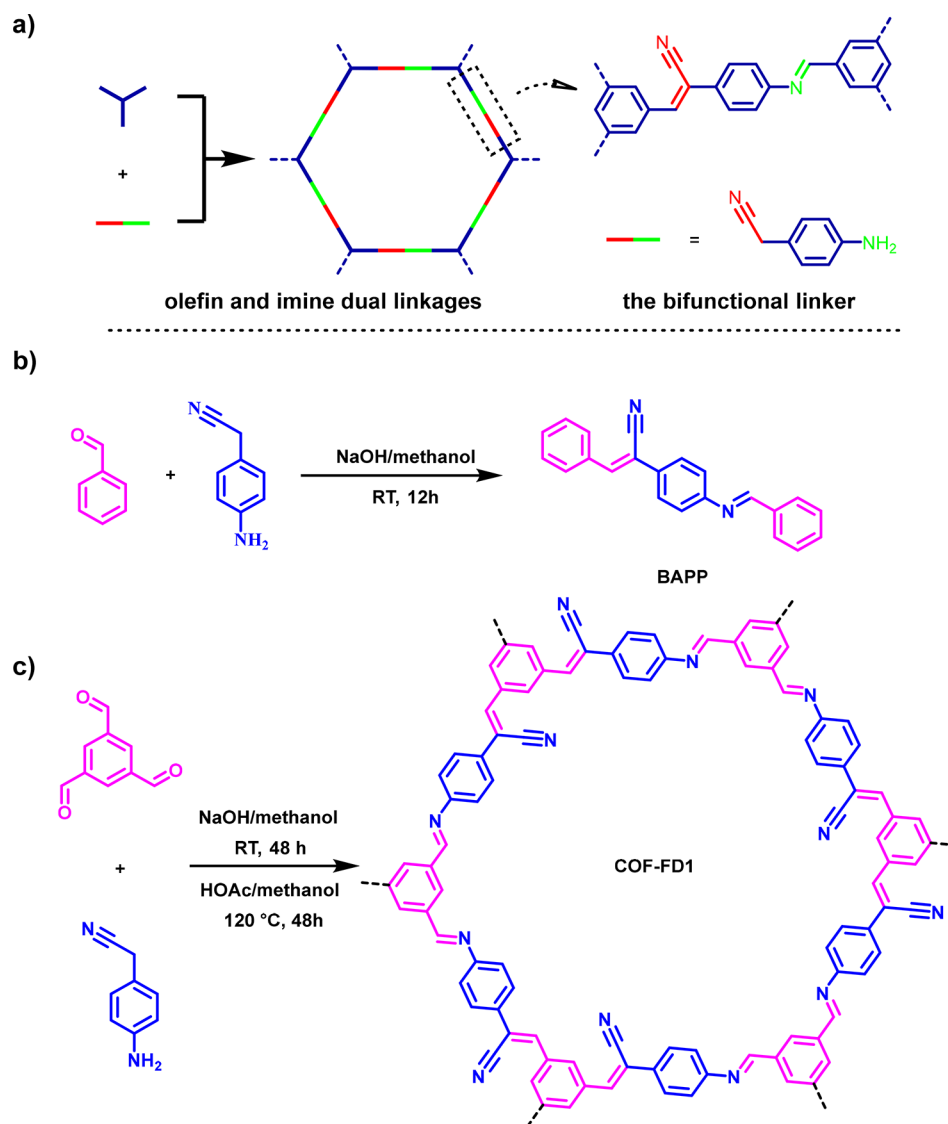
electron-withdrawing groups like nitrile could also increase the C=C bond reversibility,[65] which is a prerequisite for obtaining crystalline COFs. We thus chose benzaldehyde and 4-aminobenzyl cyanide as the model building blocks to verify the feasibility of this orthogonal reaction strategy. Encouragingly, we successfully obtained the desired molecules (BAPP) in a model reaction (Scheme 1b and Figures S1−S3), suggesting a good compatibility of the two reaction types and thus the high likelihood of constructing COFs with these dual linkages. Indeed, after extensive screening (Figures S4−S8), the use of 1,3,5-triformylbenzene (TFB) instead of benzaldehyde could finally enable us to synthesize a highly crystalline COF with olefin and imine dual linkages (Scheme 1c), which features an interesting hollow spherical morphology and exhibits remarkably high stability and excellent selectivity in fluorescence sensing of Fe^{3+} ions.

■ EXPERIMENTAL SECTION

Synthesis of (*Z*)-2-(4-{[(*E*)-Benzylidene]amino}phenyl)-3-phenylacrylonitrile (BAPP). A 10 mL Schlenk tube was charged with 4-aminobenzyl cyanide (0.132 g, 1 mmol), benzaldehyde (0.212 g, 2 mmol), and methanol (4 mL). Afterward, 0.4 mL of NaOH (4 M) was added to the mixture, and then the mixture was sonicated for 5 min; the resulting reaction mixture was allowed to stand at room temperature for 12 h, yielding BAPP (0.2684 g, 87%). ^{1}H NMR (500 MHz, chloroform-*d*): δ 8.49 (s, 1H), 7.95−7.89 (m, 4H), 7.72 (d, *J* = 8.2 Hz, 2H), 7.55 (s, 1H), 7.52−7.42 (m, 6H), 7.29 (d, *J* = 8.2 Hz, 2H). ^{13}C NMR (126 MHz, chloroform-*d*): δ 161.1, 152.9, 141.5, 136.0, 133.9, 132.1, 131.9, 130.6, 129.4, 129.1, 129.0, 127.0, 121.7, 118.1, 111.3. HRMS: *m/z* calcd for $C_{22}H_{16}N_2$ [M + H]$^+$, 309.1347; found, 309.1381. Mp: 117 °C.

Synthesis of COF-FD1. A 50 mL Schlenk tube was charged with 4-aminobenzyl cyanide (19.8 mg, 0.15 mmol) and TFB (16.2 mg, 0.1 mmol) in methanol (3 mL). Afterward, 0.4 mL of NaOH (4 M) was added to the mixture, and then the mixture was sonicated for 5 min and allowed to stand at room temperature for 2 days. Then, 0.6 mL of acetic acid (6 M) was added, and the mixture was further decompression degassed through the vacuum pump for 3 min. The
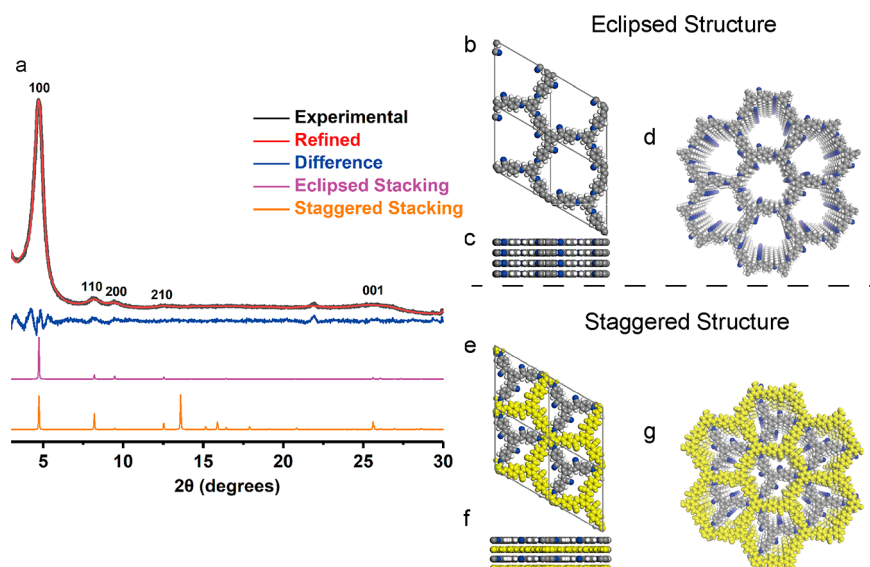
Figure 1. (a) PXRD patterns of COF-FD1 with the observed profile colored black, Pawley refinement colored red, the difference (observed minus refined) colored dark blue, simulated eclipsed stacking colored purple, and simulated staggered stacking colored orange. Eclipsed structure: views from (b and d) the *c* axis and (c) the *b* axis. Staggered structure: views from (e and g) the *c* axis and (f) the *b* axis. Gray for C, blue for N, and white for H. For the staggered structure, alternating yellow layers with undefined atoms are presented to emphasize the alternating structure.

tube was placed in an oil bath at 120 °C without disturbance for 2 days and then cooled to room temperature, and the precipitate was collected by filtration and sequentially washed twice with methanol, H_2O, DCM, and DMF. This was followed by Soxhlet extraction in THF for 24 h and drying under vacuum at 105 °C for 12 h to afford a yellow powder (25 mg, 81%).

Fluorescence Detection of Metal Ions. The metal ions used for the fluorescence sensing experiments were $SnCl_2$, $MgCl_2$, $ZnCl_2$, $CuCl_2$, $MnCl_2$, $CoCl_2 \cdot 6H_2O$, $NiCl_2$, $AlCl_3$, $CrCl_3 \cdot 6H_2O$, $FeCl_3$, and $ZrCl_4$, and the metal ion solutions (10 mM) were prepared in THF. Suspensions of COF-FD1 (1 mg/20 mL) were prepared by dispersing COF-FD1 in THF and subjecting them to ultrasonication. To explore the fluorescence response of the synthesized COF-FD1 to different metal ions in THF solutions at room temperature, 3 mL of COF-FD1 suspensions (1 mg/20 mL) was added to the cuvette (12.5 mm × 12.5 mm × 45 mm), followed by 60 μL of a blank THF or THF solution containing $M(Cl)_x$ (M^{x+} = Sn^{2+}, Mg^{2+}, Zn^{2+}, Cu^{2+}, Mn^{2+}, Co^{2+}, Ni^{2+}, Al^{3+}, Cr^{3+}, Fe^{3+}, or Zr^{4+}, 10 mM), and the fluorescence emission spectrum with an excitation wavelength of 387 nm was monitored. To further explore the selectivity of COF-FD1 for sensing Fe^{3+}, the fluorescence of the COF-FD1 suspensions (1 mg/20 mL) was investigated by testing the fluorescence intensity changes in the presence of other metal ions.

Further detailed experimental procedures and characterization are described in the Supporting Information.

■ RESULTS AND DISCUSSION

COF Synthesis and Characterizations. By screening the reaction conditions, including various different combinations of solvents and catalysts, we found that a methanol solvent and a 6 M acetic acid catalyst were more favorable for the crystallization of COF-FD1 (Figures S4–S8). Accordingly, COF-FD1 was synthesized by the reaction of 4-aminobenzyl cyanide and TFB in a methanolic NaOH solution at room temperature for 2 days, followed by the addition of an acetic acid solution and heating at 120 °C for 2 days (see the Supporting Information for details). In this synthetic strategy, an orthogonal reaction was prone to the formation of the disordered polymer framework under the catalysis of NaOH, and then the polymer framework was "self-repaired" to a highly crystalline network by adding acetic acid and heating. The

Fourier transform infrared (FT-IR) spectrum of COF-FD1 (Figure S9) shows the appearance of the C═N bond at 1624 cm^{-1} and the C≡N bond at 2218 cm^{-1}, evidencing the generation of dual linkages in the COF skeletons. These connections in the structures of COF-FD1 were further confirmed by the solid-state cross-polarization magic-angle spinning (CP/MAS) ^{13}C NMR spectrum (Figure S10). The peak at 158 ppm is attributed to the carbon atom of the C═N bond, and that at 116 ppm to the carbon atom of the C≡N bond, and the signals at 109 and 148 ppm originate from the carbon atom of the C═C bond. In addition, the signals at 127, 130, 134, 135, and 149 ppm can be assigned to the carbon atoms of the phenyl groups.[64,66]

The crystalline nature and the framework structure of COF-FD1 were elucidated by powder X-ray diffraction (PXRD) analysis in conjunction with structural simulations (Figure 1). The PXRD pattern showed a strong diffraction peak at 4.70°, accompanied by several relatively weak diffraction signals at 8.14°, 9.44°, 12.6°, and 25.8°, which can be assigned to the (100), (110), (200), (210), and (001) planes, respectively. To examine the degree of structure matching, the interlayer stacking, a geometrical energy minimization, and structural refinement by Materials Studio were conducted (see the Supporting Information for details). After Pawley refinement of the model against the experimental pattern for COF-FD1, the following unit cell parameters were generated: $a = b = 21.6031$ Å, $c = 3.1222$ Å, $\alpha = \beta = 90°$, $\gamma = 120°$, $R_{wp} = 3.29\%$, and $R_p = 2.54\%$ (Table S1 and Figure S11). As expected, the peak positions and relative intensities of the experimental and simulated PXRD pattern employing eclipsed stacking were found to be in good agreement (Figure S12). In sharp contrast, simulation of COF-FD1 with a staggered stacking mode cannot reproduce the experimental PXRD patterns (Figure S13), indicating COF-FD1 adopts an AA stacking mode. Interestingly, field emission scanning electron microscopy (FESEM) images (Figure S14) show the spherical structure of COF-FD1. The well-defined hollow spherical texture of COF-
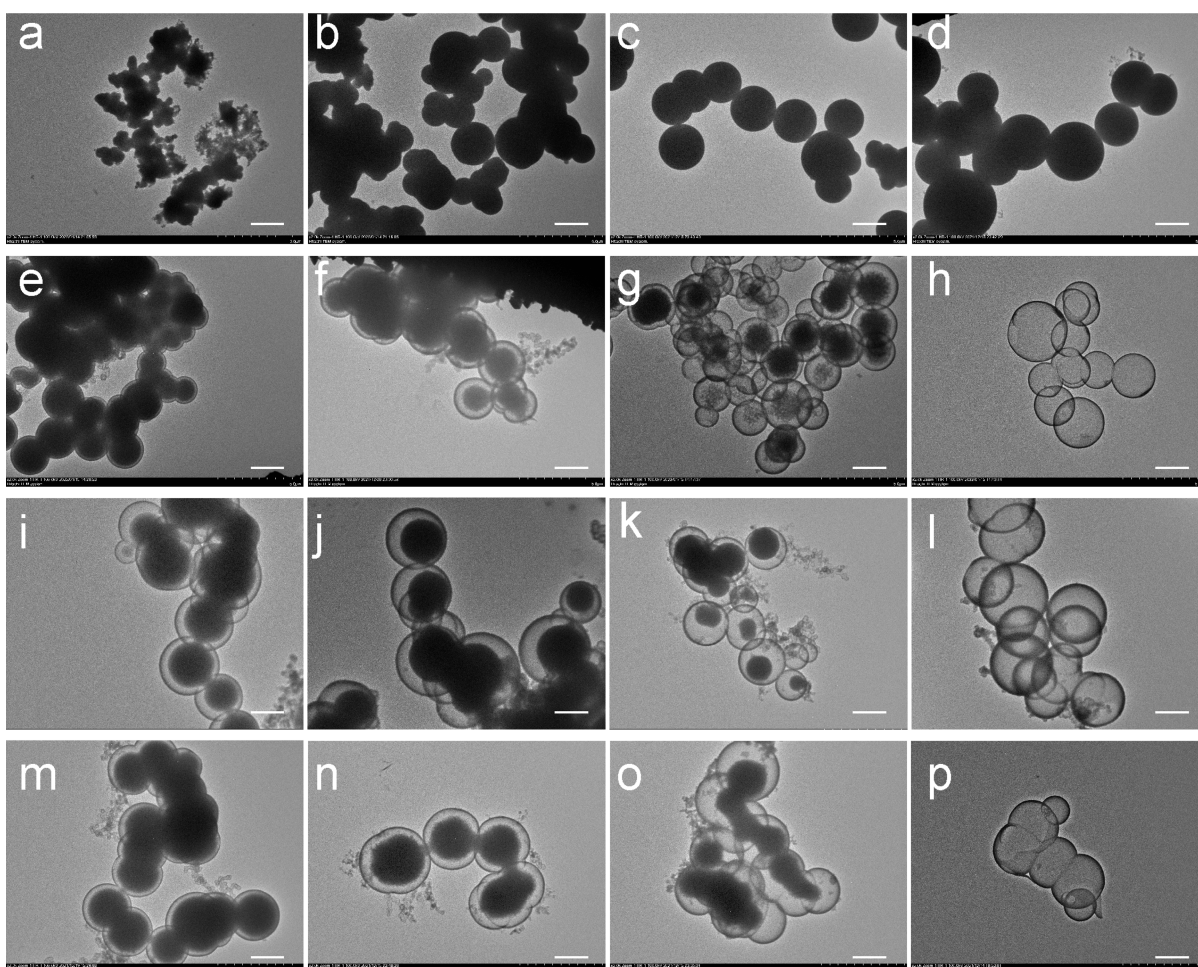
Figure 2. TEM images of COF-FD1 prepared with different times: (a) 6 h, (b) 24 h, (c) 48 h, (d) 52 h, (e, i, and m) 56 h, (f, j, and n) 64 h, (g, k, and o) 72 h, and (h, l, and p) 96 h. Scale bar of 2 μm.
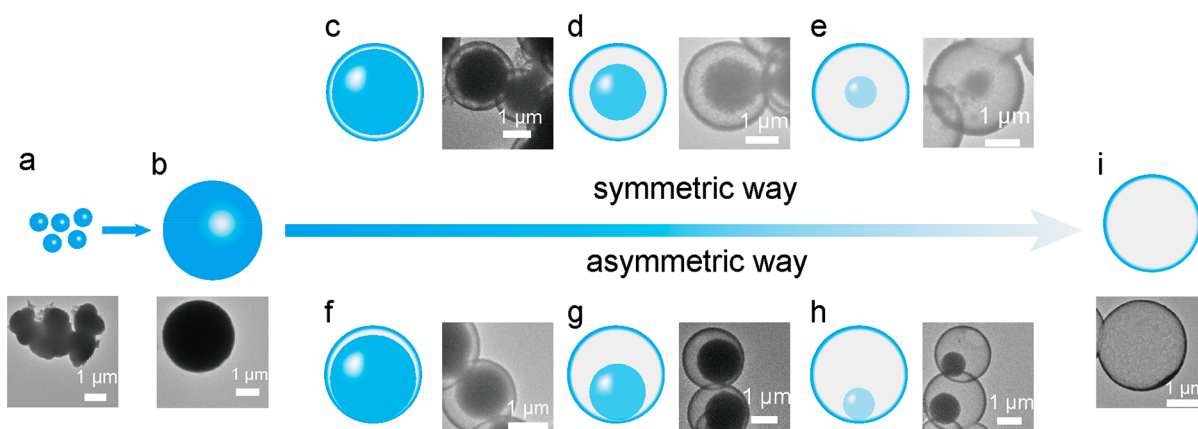

Figure 3. Hollowing evolution process of COF-FD1 via an Ostwald ripening mechanism: (a) 6 h, (b) 48 h, (c and f) 56 h, (d and g) 64 h (e and h) 72 h, and (i) 96 h.

FD1 (Figure 2 and Figure S16) was further clearly verified via transmission electron microscopy (TEM) images.

Morphology Evolution Analysis. To understand the mechanism of formation of hollow spheres, the morphological changes at different reaction times (6, 24, 48, 52, 56, 64, 72, and 96 h) were investigated by means of FESEM and TEM. With a longer reaction time, these solid spheres developed gradually and afforded a uniform spherical structure with

diameters of 2−4 μm (Figure 2a−c and Figure S14).[67] Moreover, TEM images provided clear and direct information to explore the growth pattern of these hollow spheres. After 48 h, an acid catalyst was added and the temperature was increased to 120 °C; the morphology of solid spheres remained the same until 52 h (Figure 2d). Solid evacuation started at a particular region under the surface of the solid sphere as the reaction time increased, which divided the
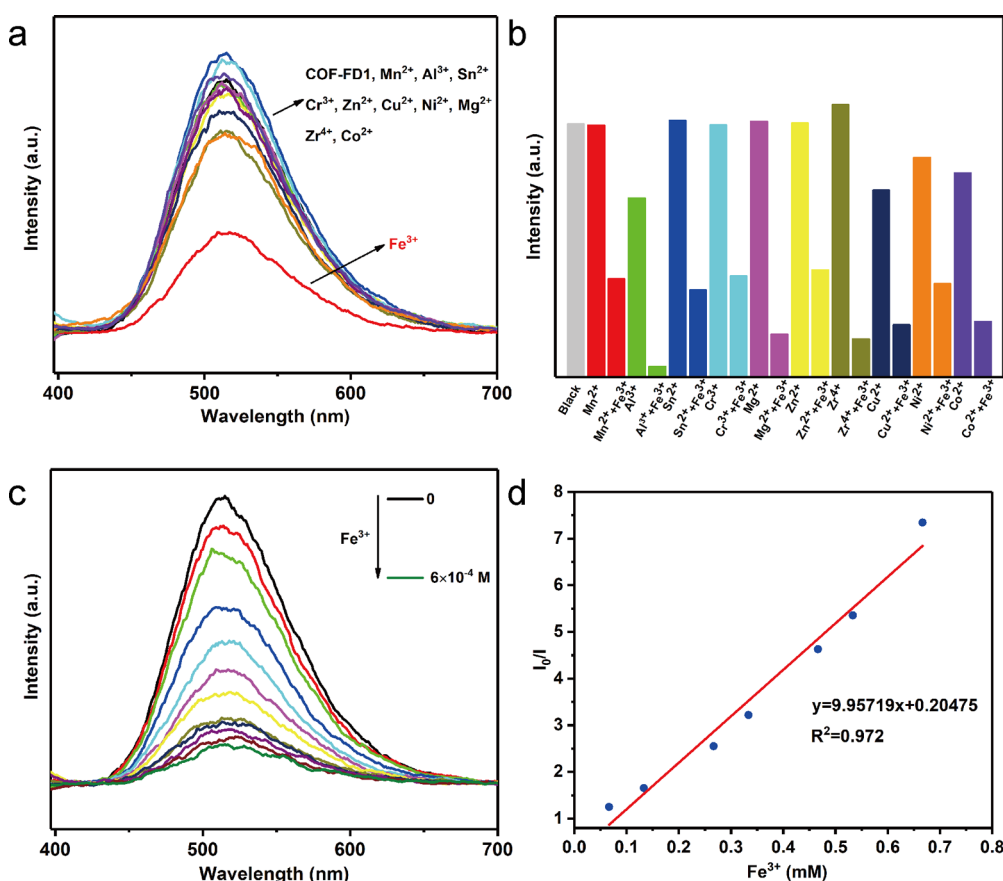
Figure 4. (a) Fluorescence emission spectra of COF-FD1 upon addition of different metal ions in THF. (b) Selectivity of COF-FD1 for sensing Fe^{3+} in THF. (c) Fluorescence titration of COF-FD1 with Fe^{3+} in THF. (d) Stern−Volmer plot of COF-FD1.

pristine solid sphere into two discrete regions and formed two core−shell hollow sphere structures, including symmetric and asymmetric core−shell hollow spheres (Figure 2e,i).[68]

Subsequently, the solid evacuation continued (Figure 2f,j), and the core was further trimmed down to a smaller size in a symmetric or an asymmetric way, leading to several symmetric or asymmetric core−shell hollow spheres (Figure 2g,k). Notably, when the reaction time reaches 96 h, the core eventually disappears thoroughly, forming a complete hollow sphere structure (Figure 2h,l). Furthermore, the fractured morphologies of the spheres were also detected by FESEM and TEM, which clearly demonstrated the shell, core−shell cavity space, and inner core of the core−shell spheres (Figure S15). In addition to most single spheres, interconnected core−shell spheres were also found (Figure 2m−p and S17). Similarly, the interconnected core−shell hollow spheres exhibited almost the same growth pattern as single spheres.[69] Meanwhile, a simultaneous enhancement in crystallinity was also observed by PXRD analysis (Figure S18), and the specific surface areas increased accordingly with a gradual hollowing of the inner cores (Figure S19), which indicates that the self-templated hollowing evolution process affects the internal ordering in the COF and the reversible "self-repair" process of COF is also used to rearrange the order of covalent bonds from random to regular order.[70] On the basis of the experimental data presented above, the solid sphere gradually transformed into a hollow sphere, in which Ostwald ripening dominated the morphological evolution with reaction time (Figure 3).[67−74]

Stability and Porosity. To our delight, by virtue of the covalent bond structures of connections, this type of COF exhibited superior stability. Thermogravimetric analysis (TGA) revealed that COF-FD1 possesses prominent thermostability with a weight loss of <4% until 400 °C under both air and nitrogen atmospheres (Figure S20). The chemical stability of COF-FD1 was investigated by PXRD after treatment for 3 days in a variety of organic solvents, such as tetrahydrofuran (THF), EtOH, N,N-dimethylformamide (DMF), dichloromethane (DCM), H_2O, and 4 M NaOH and 4 M HCl aqueous solutions. COF-FD1 exhibited good chemical stability after soaking in different solvents, evidenced by PXRD profiles (Figure S21). In particular, peaks in the PXRD pattern after water treatment were observed, suggesting this COF with dual linkages may be applied in aqueous environments. In addition, the contact-angle (CA) measurement of water on COF-FD1 revealed the relatively good hydrophilic nature of this material's surface (∼32°) (Figure S22). After its thermal stability had been determined, COF-FD1 was activated by vacuum at 105 °C for 12 h and then the integrity of the sample was confirmed by PXRD (Figure S23). The porosity of COF-FD1 was demonstrated by measuring the nitrogen adsorption−desorption isotherms at 77 K (Figure S24), giving a relatively small Brunauer−Emmett−Teller (BET) surface area of 94 m^2 g^{-1}, which may be caused by the blockage of the pore channels by large fragments or defects.[51−54] The total pore volume was calculated to be 0.089 cm^3 g^{-1} (at $P/P_0 = 0.95$), and the pore size distribution of COF-FD1 was estimated from nonlocal density functional theory (NLDFT), showing a narrow pore

width at ~1.69 nm (Figure S25a), close to the pore size predicted to be 1.85 nm from the crystal structure (Figure S25b).

Fluorescence Sensing Performances. To explore the fluorescence response of COF-FD1 to different metal ions, we dispersed COF-FD1 in different common solvents and recorded its fluorescence spectra first (Figure S26). THF, which affords the strongest fluorescence and relatively good solubility for various metal chlorides, was selected as the solvent for metal ion detection. Upon excitation at 387 nm in THF, COF-FD1 exhibited a distinct emission band at 514 nm (Figure S27). To eliminate the interference of solvents, we dissolved different $M(Cl)_x$ ions (M^{x+} = Sn^{2+}, Mg^{2+}, Zn^{2+}, Cu^{2+}, Mn^{2+}, Co^{2+}, Ni^{2+}, Al^{3+}, Cr^{3+}, Fe^{3+}, or Zr^{4+}) into THF and investigated the fluorescence sensing ability of COF-FD1 to probe metal ions in the presence of different metal ions.[75] Figure 4a shows the corresponding difference of the fluorescence intensity of COF-FD1 in THF (8×10^{-5} M) toward various metal ions (10 mM). Interestingly, the addition of metal cations such as Sn^{2+}, Mg^{2+}, Zn^{2+}, Cu^{2+}, Mn^{2+}, Co^{2+}, Ni^{2+}, Al^{3+}, Cr^{3+}, or Zr^{4+} to the suspensions led to almost no effect on the fluorescence intensity of COF-FD1. In sharp contrast, the Fe^{3+} ions induced a rapid and significant quenching effect on the fluorescence intensity in a few seconds. Notably, no distinct difference was detected in the FT-TR spectra and PXRD patterns for COF-FD1 before and after the fluorescence detection of Fe^{3+}, suggesting the robust skeleton of COF-FD1 (Figures S28 and S29). These phenomena indicate that COF-FD1 exhibits high selectivity and stability for sensing Fe^{3+} and may serve as a fluorescent sensor for detecting Fe^{3+} ions. As a control, the fluorescence detection of Fe^{3+} ions for the model compound (BAPP) was also carried out and demonstrated no fluorescence quenching under the same conditions, further proving that COF-FD1 was unique as a fluorescent sensing material (Figure S30).

To further evaluate the selectivity of COF-FD1 for sensing Fe^{3+}, comparative experiments were performed by mixing COF-FD1 suspensions with Fe^{3+} and other metal ions, and the results are depicted in Figure 4b. It was found that the interference of most metal ions has led to an only minor influence on the detection of Fe^{3+} by COF-FD1, which also clarifies that COF-FD1 has a high selectivity for sensing Fe^{3+}.

Sensitivity is another critical feature of effective fluorescent sensors. To examine the sensitivity of COF-FD1 to Fe^{3+}, fluorescence titration experiments were conducted. As displayed in Figure 4c, the fluorescence intensity of COF-FD1 exhibits a sharp decrease with an increase in Fe^{3+} ion concentration from 3×10^{-5} to 6×10^{-4} M. To qualitatively describe the quenching sensitivity, we evaluated the values of the quenching coefficient of Fe^{3+} for the fluorescence of COF-FD1 by using the Stern–Volmer equation: $I_0/I = 1 + K_{SV}[M]$ (where I_0 and I represent the fluorescence intensities of COF-FD1 in the absence and presence of the Fe^{3+} ion, respectively, K_{SV} is the quenching coefficient, and $[M]$ is the concentration of the Fe^{3+} ion).[76] A good linear Stern–Volmer relationship was observed for COF-FD1, and the quenching coefficient is estimated to be 9.957×10^3 M^{-1}, as described in Figure 4d. In addition, the limit of detection (LOD) of COF-FD1 for fluorescence sensing of Fe^{3+} was obtained from the formula LOD = $3\sigma/K_{SV}$ (σ is the standard deviation of the blank solution, and K_{SV} is the slope of the Stern–Volmer graph),[77] and the low LOD of COF-FD1 was calculated to be ~6.39 μM, representing an excellent sensitivity for Fe^{3+} detection.

To explore the possible mechanism of COF-FD1 for Fe^{3+} detection, the ultraviolet–visible (UV–vis) absorption spectra of BAPP (Figure S31), the COF-FD1 suspension, and all metal ions in THF solutions are illustrated in Figure 5, showing that
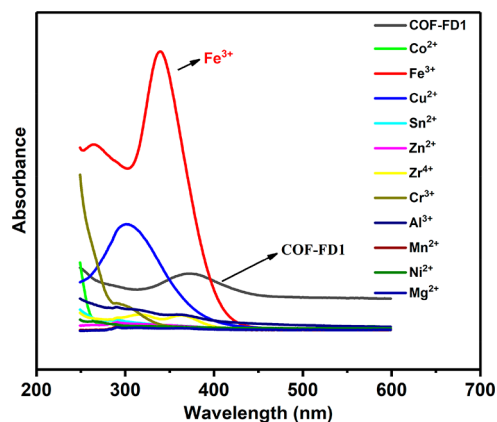

Figure 5. UV–vis absorption spectra of metal ions and COF-FD1 in a THF solution.

Fe^{3+} displays a higher and more obvious absorption peak at 300–400 nm, while other metal ions (Sn^{2+}, Mg^{2+}, Zn^{2+}, Cu^{2+}, Mn^{2+}, Co^{2+}, Ni^{2+}, Al^{3+}, Cr^{3+}, and Zr^{4+}) have only very weak or no pronounced absorption peaks; the absorption spectrum of Fe^{3+} also exhibits a more considerable overlap with that of COF-FD1, while other metal ions do not. Both COF-FD1 and Fe^{3+} represent a strong absorption centered at ~387 nm, but the absorption of Fe^{3+} is much greater than that of COF-FD1, suggesting a strong absorption competition of the light source energy between COF-FD1 and Fe^{3+}. The Fe^{3+} filters the light absorbed by COF-FD1, thus resulting in fluorescence quenching, implying an absorption competitive quenching (ACQ) mechanism.[78−81]

■ CONCLUSIONS

In summary, we have developed a new strategy for constructing a COF with dual linkages by orthogonal Schiff base reaction and the Knoevenagel condensation reaction, which enables the synthesis of a new type of hollow spherical COF with olefin and imine dual linkages for the first time. COF-FD1 crystallites self-assembled into hollow spheres, and the continuous transformation process from initial solid spherical into hollow spherical structure was studied by TEM, FESEM, PXRD, and N_2 sorption analysis and revealed in accord with the Ostwald ripening mechanism. Remarkably, COF-FD1 exhibited outstanding thermal and chemical stability and showed its good potential in fluorescence sensing with excellent selectivity toward Fe^{3+} ions. So far, the development of COFs with dual linkages is still limited, and the successful preparation of COF with olefin and imine dual linkages in this study suggests the strategy developed could not only provide a possible pathway for synthesizing COFs with hollow structures, or even more complex structures and compositions, but also potentially expand the types and quantities of COFs.

■ ASSOCIATED CONTENT

ⓈI Supporting Information

The Supporting Information is available free of charge at https://pubs.acs.org/doi/10.1021/acs.chemmater.2c00922.

Materials, instrumentation, synthetic procedures, FT-IR spectra, PXRD patterns, ^{13}C CP/MAS NMR spectra, details of the structural simulation, FESEM images, TEM images, TGA, chemical stability analysis, N$_2$ sorption isotherms, pore size distribution, and fluorescence spectra (PDF)

■ AUTHOR INFORMATION

Corresponding Authors

Lili Xie − *Key Laboratory of Molecule Synthesis and Function Discovery (Fujian Province University), State Key Laboratory of Photocatalysis on Energy and Environment, College of Chemistry, Fuzhou University, Fuzhou 350108, China;* Email: xielili@fzu.edu.cn

Xiong Chen − *Key Laboratory of Molecule Synthesis and Function Discovery (Fujian Province University), State Key Laboratory of Photocatalysis on Energy and Environment, College of Chemistry, Fuzhou University, Fuzhou 350108, China;* ⊙ orcid.org/0000-0003-2878-7522; Email: chenxiong987@fzu.edu.cn

Authors

Jingtao Hu − *Key Laboratory of Molecule Synthesis and Function Discovery (Fujian Province University), State Key Laboratory of Photocatalysis on Energy and Environment, College of Chemistry, Fuzhou University, Fuzhou 350108, China*

Junjie Zhang − *Key Laboratory for Analytical Science of Food Safety and Biology (Ministry of Education), College of Chemistry, Fuzhou University, Fuzhou 350108, China*

Zhangxiang Lin − *Qingyuan Innovation Laboratory, Quanzhou 362801, China*

Saihu Liao − *Key Laboratory of Molecule Synthesis and Function Discovery (Fujian Province University), State Key Laboratory of Photocatalysis on Energy and Environment, College of Chemistry, Fuzhou University, Fuzhou 350108, China;* ⊙ orcid.org/0000-0002-0251-8757

Complete contact information is available at:
https://pubs.acs.org/10.1021/acs.chemmater.2c00922

Notes

The authors declare no competing financial interest.

■ REFERENCES

(1) Cote, A. P.; Benin, A. I.; Ockwig, N. W.; O'Keeffe, M.; Matzger, A. J.; Yaghi, O. M. Porous, crystalline, covalent organic frameworks. *Science* **2005**, *310*, 1166−1170.

(2) El-Kaderi, H. M.; Hunt, J. R.; Mendoza-Cortes, J. L.; Cote, A. P.; Taylor, R. E.; O'Keeffe, M.; Yaghi, O. M. Designed synthesis of 3D covalent organic frameworks. *Science* **2007**, *316*, 268−272.

(3) Uribe-Romo, F. J.; Hunt, J. R.; Furukawa, H.; Klock, C.; O'Keeffe, M.; Yaghi, O. M. A Crystalline Imine-Linked 3-D Porous Covalent Organic Framework. *J. Am. Chem. Soc.* **2009**, *131*, 4570−4571.

(4) Colson, J. W.; Woll, A. R.; Mukherjee, A.; Levendorf, M. P.; Spitler, E. L.; Shields, V. B.; Spencer, M. G.; Park, J.; Dichtel, W. R. Oriented 2D Covalent Organic Framework Thin Films on Single-Layer Graphene. *Science* **2011**, *332*, 228−231.

(5) Ma, T.; Kapustin, E. A.; Yin, S. X.; Liang, L.; Zhou, Z.; Niu, J.; Li, L.; Wang, Y.; Su, J.; Li, J.; Wang, X.; Wang, W. D.; Wang, W.; Sun, J.; Yaghi, O. M. Single-Crystal X-Ray Diffraction Structures of Covalent Organic Frameworks. *Science* **2018**, *361*, 48−52.

(6) Parent, L. R.; Flanders, N. C.; Bisbey, R. P.; Vitaku, E.; Evans, A. M.; Kirschner, M. S.; Schaller, R. D.; Chen, L. X.; Gianneschi, N. C.; Dichtel, W. R. Seeded Growth of Single-Crystal Two-Dimensional Covalent Organic Frameworks. *Science* **2018**, *361*, 52−57.

(7) Wan, S.; Guo, J.; Kim, J.; Ihee, H.; Jiang, D. A Photoconductive Covalent Organic Framework: Self-Condensed Arene Cubes Composed of Eclipsed 2D Polypyrene Sheets for Photocurrent Generation. *Angew. Chem., Int. Ed.* **2009**, *121*, 5547−5550.

(8) Huang, W.; Jiang, Y.; Li, X.; Li, X. J.; Wang, J. Y.; Wu, Q.; Liu, X. K. Solvothermal Synthesis of Microporous, Crystalline Covalent Organic Framework Nanofibers and Their Colorimetric Nanohybrid Structures. *ACS Appl. Mater. Interfaces* **2013**, *5*, 8845−8849.

(9) Chandra, S.; Kandambeth, S.; Biswal, B. P.; Lukose, B.; Kunjir, S. M.; Chaudhary, M.; Babarao, R.; Heine, T.; Banerjee, R. Chemically Stable Multilayered Covalent Organic Nanosheets from Covalent Organic Frameworks via Mechanical Delamination. *J. Am. Chem. Soc.* **2013**, *135*, 17853−17861.

(10) Li, B. Q.; Zhang, S. Y.; Kong, L.; Peng, H. J.; Zhang, Q. Porphyrin Organic Framework Hollow Spheres and Their Applications in Lithium-Sulfur Batteries. *Adv. Mater.* **2018**, *30*, 1707483.

(11) Ma, W.; Zheng, Q.; He, Y.; Li, G.; Guo, W.; Lin, Z.; Zhang, L. Size-Controllable Synthesis of Uniform Spherical Covalent Organic Frameworks at Room Temperature for Highly Efficient and Selective Enrichment of Hydrophobic Peptides. *J. Am. Chem. Soc.* **2019**, *141*, 18271−18277.

(12) Li, Y.; Wu, S.; Zhang, L.; Xu, X.; Fang, Y.; Yi, J.; Kim, J.; Shen, B.; Lee, M.; Huang, L.; Zhang, L.; Bao, J.; Ji, H.; Huang, Z. Precisely Controlled Multidimensional Covalent Frameworks: Polymerization of Supramolecular Colloids. *Angew. Chem., Int. Ed.* **2020**, *59*, 21525−21529.

(13) Xiong, Z.; Sun, B.; Zou, H.; Wang, R.; Fang, Q.; Zhang, Z.; Qiu, S. Amorphous-to-Crystalline Transformation: General Synthesis of Hollow Structured Covalent Organic Frameworks with High Crystallinity. *J. Am. Chem. Soc.* **2022**, *144*, 6583−6593.

(14) Chen, X.; Addicoat, M.; Irle, S.; Nagai, A.; Jiang, D. Control Crystallinity and Porosity of Covalent Organic Frameworks through Managing Interlayer Interactions Based on Self-Complementary π-Electronic Force. *J. Am. Chem. Soc.* **2013**, *135*, 546−549.

(15) Chen, X.; Addicoat, M.; Jin, E.; Zhai, L.; Xu, H.; Huang, N.; Guo, Z.; Liu, L.; Irle, S.; Jiang, D. Locking Covalent Organic Frameworks with Hydrogen Bonds: General and Remarkable Effects on Crystalline Structure, Physical Properties, and Photochemical Activities. *J. Am. Chem. Soc.* **2015**, *137*, 3241−3247.

(16) Martinez-Abadia, M.; Mateo-Alonso, A. Structural Approaches to Control Interlayer Interactions in 2D Covalent Organic Frameworks. *Adv. Mater.* **2020**, *32*, 2002366.

(17) Segura, J. L.; Mancheno, M. J.; Zamora, F. Covalent Organic Frameworks Based on Schiff-Base Chemistry: Synthesis, Properties and Potential Applications. *Chem. Soc. Rev.* **2016**, *45*, 5635−5671.

(18) Nguyen, H. L.; Gropp, C.; Yaghi, O. M. Reticulating 1D Ribbons into 2D Covalent Organic Frameworks by Imine and Imide Linkages. *J. Am. Chem. Soc.* **2020**, *142*, 2771−2776.

(19) Feng, X.; Ding, X.; Jiang, D. Covalent organic frameworks. *Chem. Soc. Rev.* **2012**, *41*, 6010−6022.

(20) Liu, R.; Tan, K. T.; Gong, Y.; Chen, Y.; Li, Z.; Xie, S.; He, T.; Lu, Z.; Yang, H.; Jiang, D. Covalent Organic Frameworks: An Ideal Platform for Designing Ordered Materials and Advanced Applications. *Chem. Soc. Rev.* **2021**, *50*, 120−242.

(21) Furukawa, H.; Yaghi, O. M. Storage of Hydrogen, Methane, and Carbon Dioxide in Highly Porous Covalent Organic Frameworks for Clean Energy Applications. *J. Am. Chem. Soc.* **2009**, *131*, 8875−8883.

(22) Doonan, C. J.; Tranchemontagne, D. J.; Glover, T. G.; Hunt, J. R.; Yaghi, O. M. Exceptional Ammonia Uptake by a Covalent Organic Framework. *Nat. Chem.* **2010**, *2*, 235−238.

(23) Guan, X.; Ma, Y.; Li, H.; Yusran, Y.; Xue, M.; Fang, Q.; Yan, Y.; Valtchev, V.; Qiu, S. Fast, Ambient Temperature and Pressure Ionothermal Synthesis of Three-Dimensional Covalent Organic Frameworks. *J. Am. Chem. Soc.* **2018**, *140*, 4494−4498.

(24) Xu, H.; Chen, X.; Gao, J.; Lin, J.; Addicoat, M.; Irle, S.; Jiang, D. Catalytic Covalent Organic Frameworks via Pore Surface Engineering. *Chem. Commun.* **2014**, *50*, 1292−1294.

(25) Han, X.; Yuan, C.; Hou, B.; Liu, L.; Li, H.; Liu, Y.; Cui, Y. Chiral Covalent Organic Frameworks: Design, Synthesis and Property. *Chem. Soc. Rev.* **2020**, *49*, 6248−6272.

(26) He, C.; Liang, J.; Zou, Y. H.; Yi, J. D.; Huang, Y. B.; Cao, R. Metal-Organic Frameworks Bonded with Metal N-Heterocyclic Carbenes for efficient catalysis. *Natl. Sci. Rev.* **2021**, nwab157.

(27) Nagai, A.; Chen, X.; Feng, X.; Ding, X.; Guo, Z.; Jiang, D. A Squaraine-Linked Mesoporous Covalent Organic Framework. *Angew. Chem., Int. Ed.* **2013**, *52*, 3770−3774.

(28) Stegbauer, L.; Schwinghammer, K.; Lotsch, B. V. A Hydrazone-Based Covalent Organic Framework for Photocatalytic Hydrogen Production. *Chem. Sci.* **2014**, *5*, 2789−2793.

(29) Bi, S.; Yang, C.; Zhang, W.; Xu, J.; Liu, L.; Wu, D.; Wang, X.; Han, Y.; Liang, Q.; Zhang, F. Two-dimensional semiconducting covalent organic frameworks via condensation at arylmethyl carbon atoms. *Nat. Commun.* **2019**, *10*, 2467.

(30) Li, Z.; Zhi, Y.; Shao, P.; Xia, H.; Li, G.; Feng, X.; Chen, X.; Shi, Z.; Liu, X. Covalent Organic Framework as an Efficient, Metal-free, Heterogeneous Photocatalyst for Organic Transformations under Visible Light. *Appl. Catal. B: Environ.* **2019**, *245*, 334−342.

(31) Chen, W.; Wang, L.; Mo, D.; He, F.; Wen, Z.; Wu, X.; Xu, H.; Chen, L. Modulating Benzothiadiazole-Based Covalent Organic Frameworks via Halogenation for Enhanced Photocatalytic Water Splitting: Small Changes Make Big Differences. *Angew. Chem., Int. Ed.* **2020**, *59*, 16902−16909.

(32) Guo, J.; Jiang, D. Covalent Organic Frameworks for Heterogeneous Catalysis: Principle, Current Status, and Challenges. *ACS Central Sci.* **2020**, *6*, 869−879.

(33) DeBlase, C. R.; Silberstein, K. E.; Truong, T.; Abruña, H. D.; Dichtel, W. R. β-Ketoenamine-Linked Covalent Organic Frameworks Capable of Pseudocapacitive Energy Storage. *J. Am. Chem. Soc.* **2013**, *135*, 16821−16824.

(34) Xu, F.; Xu, H.; Chen, X.; Wu, D.; Wu, Y.; Liu, H.; Gu, C.; Fu, R.; Jiang, D. Radical Covalent Organic Frameworks: A General Strategy to Immobilize Open-Accessible Polyradicals and High-Performance Capacitive Energy Storage. *Angew. Chem., Int. Ed.* **2015**, *54*, 6814−6818.

(35) Luo, Z. Q.; Liu, L. J.; Ning, J. X.; Lei, K. X.; Lu, Y.; Li, F. J.; Chen, J. A Microporous Covalent-Organic Framework with Abundant Accessible Carbonyl Groups for Lithium-Ion Batteries. *Angew. Chem., Int. Ed.* **2018**, *57*, 9443−9446.

(36) Xu, F.; Yang, S.; Chen, X.; Liu, Q.; Li, H.; Wang, H.; Wei, B.; Jiang, D. Energy-Storage Covalent Organic Frameworks: Improving Performance via Engineering Polysulfide Chains on Walls. *Chem. Sci.* **2019**, *10*, 6001−6006.

(37) Tao, S.; Jiang, D. Covalent Organic Frameworks for Energy Conversions: Current Status, Challenges, and Perspectives. *CCS Chem.* **2021**, *3*, 2003−2024.

(38) Wang, C.; Zhang, Z.; Zhu, Y.; Yang, C.; Wu, J.; Hu, W. 2D Covalent Organic Frameworks: From Synthetic Strategies to Advanced Optical-Electrical-Magnetic Functionalities. *Adv. Mater.* **2022**, *34*, 2102290.

(39) Wu, Q.; Xie, R. K.; Mao, M. J.; Chai, G. L.; Yi, J. D.; Zhao, S. S.; Huang, Y. B.; Cao, R. Integration of Strong Electron Transporter Tetrathiafulvalene into Metalloporphyrin-Based Covalent Organic Framework for Highly Efficient Electroreduction of CO_2. *ACS Energy Lett.* **2020**, *5*, 1005−1012.

(40) Zhang, M. D.; Si, D. H.; Yi, J. D.; Zhao, S. S.; Huang, Y. B.; Cao, R. Conductive Phthalocyanine-Based Covalent Organic Framework for Highly Efficient Electroreduction of Carbon Dioxide. *Small* **2020**, *16*, 2005254.

(41) Meng, D. L.; Zhang, M. D.; Si, D. H.; Mao, M. J.; Hou, Y.; Huang, Y. B.; Cao, R. Highly Selective Tandem Electroreduction of CO_2 to Ethylene over Atomically Isolated Nickel-Nitrogen Site/ Copper Nanoparticle Catalysts. *Angew. Chem., Int. Ed.* **2021**, *60*, 25485−25492.

(42) Hou, Y.; Huang, Y.-B.; Liang, Y. L.; Chai, G. L.; Yi, J. D.; Zhang, T.; Zang, K. T.; Luo, J.; Xu, R.; Lin, H.; Zhang, S. Y.; Wang, H. M.; Cao, R. Unraveling the Reactivity and Selectivity of Atomically Isolated Metal−Nitrogen Sites Anchored on Porphyrinic Triazine Frameworks for Electroreduction of CO_2. *CCS Chem.* **2019**, *1*, 384−395.

(43) Yusran, Y.; Guan, X.; Li, H.; Fang, Q.; Qiu, S. Postsynthetic Functionalization of Covalent Organic Frameworks. *Natl. Sci. Rev.* **2020**, *7*, 170−190.

(44) Ding, S. Y.; Dong, M.; Wang, Y. W.; Chen, Y. T.; Wang, H. Z.; Su, C. Y.; Wang, W. Thioether-Based Fluorescent Covalent Organic Framework for Selective Detection and Facile Removal of Mercury (II). *J. Am. Chem. Soc.* **2016**, *138*, 3031−3037.

(45) Li, Z.; Zhang, Y.; Xia, H.; Mu, Y.; Liu, X. A Robust and Luminescent Covalent Organic Framework as a Highly Sensitive and Selective Sensor for the Detection of Cu^{2+} ions. *Chem.Commun.* **2016**, *52*, 6613−6616.

(46) Ascherl, L.; Evans, E. W.; Gorman, J.; Orsborne, S.; Bessinger, D.; Bein, T.; Friend, R. H.; Auras, F. Perylene-Based Covalent Organic Frameworks for Acid Vapor Sensing. *J. Am. Chem. Soc.* **2019**, *141*, 15693−15699.

(47) Jiang, S.; Meng, L.; Ma, W.; Pan, G.; Zhang, W.; Zou, Y.; Liu, L.; Xu, B.; Tian, W. Dual-Functional Two-Dimensional Covalent Organic Frameworks for Water Sensing and Harvesting. *Mater. Chem. Front.* **2021**, *5*, 4193−4201.

(48) Zeng, J. Y.; Wang, X. S.; Zhang, X. Z. Research Progress in Covalent Organic Frameworks for Photoluminescent Materials. *Chem. - Eur. J.* **2020**, *26*, 16568−16581.

(49) Skorjanc, T.; Shetty, D.; Valant, M. Covalent Organic Polymers and Frameworks for Fluorescence-Based Sensors. *ACS Sens.* **2021**, *6*, 1461−1481.

(50) Guo, L.; Yang, L.; Li, M.; Kuang, L.; Song, Y.; Wang, L. Covalent Organic Frameworks for Fluorescent Sensing: Recent Developments and Future Challenges. *Coord. Chem. Reviw.* **2021**, *440*, 213957.

(51) Xu, J.; Yang, C.; Bi, S.; Wang, W.; He, Y.; Wu, D.; Liang, Q.; Wang, X.; Zhang, F. Vinylene-Linked Covalent Organic Frameworks (COFs) with Symmetry-Tuned Polarity and Photocatalytic Activity. *Angew. Chem., Int. Ed.* **2020**, *59*, 23845−23853.

(52) Geng, K. Y.; He, T.; Liu, R. Y.; Dalapati, S.; Tan, K. T.; Li, Z. P.; Tao, S. S.; Gong, Y. F.; Jiang, Q. H.; Jiang, D. Covalent Organic Frameworks: Design, Synthesis, and Functions. *Chem. Rev.* **2020**, *120*, 8814−8933.

(53) Ji, C.; Su, K.; Wang, W.; Chang, J.; El-Sayed, E. S. M.; Zhang, L.; Yuan, D. Tunable Cage-Based Three-Dimensional Covalent Organic Frameworks. *CCS Chem.* **2021**, *3*, 3094−3104.

(54) Guo, L.; Zhang, J.; Huang, Q.; Zhou, W.; Jin, S. Progress in Synthesis of Highly Crystalline Covalent Organic Frameworks and Their Crystallinity Enhancement Strategies. *Chin. Chem. Lett.* **2022**, *33*, 2856−2866.

(55) Hu, J. Y.; Gupta, S. K.; Ozdemir, J.; Beyzavi, M. H. Applications of Dynamic Covalent Chemistry Concept toward Tailored Covalent Organic Framework Nanomaterials: A Review. *ACS Appl. Nano Mater.* **2020**, *3*, 6239−6269.

(56) Zeng, Y. F.; Zou, R. Y.; Luo, Z.; Zhang, H. C.; Yao, X.; Ma, X.; Zou, R. Q.; Zhao, Y. L. Covalent Organic Frameworks Formed with Two Types of Covalent Bonds Based on Orthogonal Reactions. *J. Am. Chem. Soc.* **2015**, *137*, 1020−1023.

(57) Liang, R. R.; A, R.-H.; Xu, S. Q.; Qi, Q. Y.; Zhao, X. Fabricating Organic Nanotubes through Selective Disassembly of Two-Dimensional Covalent Organic Frameworks. *J. Am. Chem. Soc.* **2020**, *142*, 70−74.

(58) Xiao, Z. B.; Li, L. Y.; Tang, Y. J.; Cheng, Z. B.; Pan, H.; Tian, D. X.; Wang, R. H. Covalent Organic Frameworks with Lithiophilic and

Sulfiphilic Dual Linkages for Cooperative Affinity to Polysulfides in Lithium-Sulfur Batteries. *Energy Storage Mater.* **2018**, *12*, 252−259.

(59) Yue, J. Y.; Mo, Y. P.; Li, S. Y.; Dong, W. L.; Chen, T.; Wang, D. Simultaneous Construction of Two Linkages for the On-Surface Synthesis of Imine-Boroxine Hybrid Covalent Organic Frameworks. *Chem. Sci.* **2017**, *8*, 2169−2174.

(60) Chen, X.; Addicoat, M.; Jin, E. Q.; Xu, H.; Hayashi, T.; Xu, F.; Huang, N.; Irle, S.; Jiang, D. Designed Synthesis of Double-Stage Two-Dimensional Covalent Organic Frameworks. *Sci. Rep.* **2015**, *5*, 14650.

(61) Li, H. Q.; Qi, Q. Y.; Zhao, X.; Li, G.; Chen, X.; Zhang, H. J.; Lin, J. Synthesis of Novel 2D In-Plane Anisotropic Covalent Organic Frameworks through a Solvent Modulated Orthogonal Strategy. *Polym. Chem.* **2018**, *9*, 4288−4293.

(62) Li, H.; Pan, Q.; Ma, Y.; Guan, X.; Xue, M.; Fang, Q.; Yan, Y.; Valtchev, V.; Qiu, S. Three-Dimensional Covalent Organic Frameworks with Dual Linkages for Bifunctional Cascade Catalysis. *J. Am. Chem. Soc.* **2016**, *138*, 14783−14788.

(63) Liang, R. R.; Xu, S. Q.; Pang, Z. F.; Qi, Q. Y.; Zhao, X. Self-Sorted Pore-Formation in the Construction of Heteropore Covalent Organic Frameworks Based on Orthogonal Reactions. *Chem. Commun.* **2018**, *54*, 880−883.

(64) Ding, S. Y.; Gao, J.; Wang, Q.; Zhang, Y.; Song, W. G.; Su, C. Y.; Wang, W. Construction of Covalent Organic Framework for Catalysis: Pd/COF-LZU1 in Suzuki-Miyaura Coupling Reaction. *J. Am. Chem. Soc.* **2011**, *133*, 19816−19822.

(65) Lyu, H.; Diercks, C. S.; Zhu, C. H.; Yaghi, O. M. Porous Crystalline Olefin-Linked Covalent Organic Frameworks. *J. Am. Chem. Soc.* **2019**, *141*, 6848−6852.

(66) Wang, S.; Li, X. X.; Da, L.; Wang, Y.; Xiang, Z.; Wang, W.; Zhang, Y. B.; Cao, D. A Three-Dimensional sp^2 Carbon-Conjugated Covalent Organic Framework. *J. Am. Chem. Soc.* **2021**, *143*, 15562−15566.

(67) Liu, Y. Y.; Li, X. C.; Wang, S.; Cheng, T.; Yang, H. Y.; Liu, C.; Gong, Y. T.; Lai, W. Y.; Huang, W. Self-Templated Synthesis of Uniform Hollow Spheres Based on Highly Conjugated Three-Dimensional Covalent Organic Frameworks. *Nat. Commun.* **2020**, *11*, 5561.

(68) Liu, B.; Zeng, H. C. Symmetric and Asymmetric Ostwald Ripening in the Fabrication of Homogeneous Core−Shell Semiconductors. *Small* **2005**, *1*, 566−571.

(69) Mao, B.; Guo, D.; Qin, J.; Meng, T.; Wang, X.; Cao, M. Solubility-Parameter-Guided Solvent Selection to Initiate Ostwald Ripening for Interior Space-Tunable Structures with Architecture-Dependent Electrochemical Performance. *Angew. Chem., Int. Ed.* **2018**, *57*, 596−596.

(70) Kandambeth, S.; Venkatesh, V.; Shinde, D. B.; Kumari, S.; Halder, A.; Verma, S.; Banerjee, R. Self-Templated Chemically Stable Hollow Spherical Covalent Organic Framework. *Nat. Commun.* **2015**, *6*, 6786.

(71) Tian, X.; Li, J.; Chen, K.; Han, J.; Pan, S.; Wang, Y.; Fan, X.; Li, F.; Zhou, Z. Nearly Monodisperse Ferroelectric BaTiO3 Hollow Nanoparticles: Size-Related Solid Evacuation in Ostwald-Ripening-Induced Hollowing Process. *Cryst. Growth Des.* **2010**, *10*, 3990−3995.

(72) Xie, J. F.; Zhang, X. D.; Zhang, H.; Zhang, J. J.; Li, S.; Wang, R. X.; Pan, B. C.; Xie, Y. Intralayered Ostwald Ripening to Ultrathin Nanomesh Catalyst with Robust Oxygen-Evolving Performance. *Adv. Mater.* **2017**, *29*, 1604765.

(73) Shen, L. F.; Yu, L.; Yu, X. Y.; Zhang, X. G.; Lou, X. W. Self-Templated Formation of Uniform NiCo2O4 Hollow Spheres with Complex Interior Structures for Lithium-Ion Batteries and Supercapacitors. *Angew. Chem., Int. Ed.* **2015**, *54*, 1868−1872.

(74) Tian, X.; Li, J.; Chen, K.; Han, J.; Pan, S. Template-Free and Scalable Synthesis of Core−Shell and Hollow BaTiO3 Particles: Using Molten Hydrated Salt as a Solvent. *Cryst. Growth Des.* **2009**, *9*, 4927−4932.

(75) Özdemir, E.; Thirion, D.; Yavuz, C. T. Covalent Organic Polymer Framework with C−C Bonds as a Fluorescent Probe for Selective Iron Detection. *RSC Adv.* **2015**, *5*, 69010−69015.

(76) Li, Y. J.; Han, Y. N.; Chen, M. H.; Feng, Y. Q.; Zhang, B. Construction of a Flexible Covalent Organic Framework Based on Triazine Units with Interesting Photoluminescent Properties for Sensitive and Selective Detection of Picric Acid. *RSC Adv.* **2019**, *9*, 30937−30942.

(77) Mangalath, S.; Abraham, S.; Joseph, J. pH-Responsive Fluorescence Enhancement in Graphene Oxide−Naphthalimide Nanoconjugates: A Fluorescence Turn-On Sensor for Acetylcholine. *Chem. - Eur. J.* **2017**, *23*, 11404−11409.

(78) Li, Y. J.; Chen, M. H.; Han, Y. N.; Feng, Y. Q.; Zhang, Z. J.; Zhang, B. Fabrication of a New Corrole-Based Covalent Organic Framework as a Highly Efficient and Selective Chemosensor for Heavy Metal Ions. *Chem. Mater.* **2020**, *32*, 2532−2540.

(79) Wang, M.; Guo, L.; Cao, D. Porous organic polymer nanotubes as luminescent probe for highly selective and sensitive detection of Fe^{3+}. *Sci. China Chem.* **2017**, *60*, 1090−1097.

(80) Guo, L.; Zeng, X. F.; Lan, J. H.; Yun, J.; Cao, D. P. Absorption Competition Quenching Mechanism of Porous Covalent Organic Polymer as Luminescent Sensor for Selective Sensing Fe^{3+}. *ChemistrySelect* **2017**, *2*, 1041−1047.

(81) Zhou, Y.; Chen, H.; Yan, B. An Eu^{3+} Post-Functionalized Nanosized Metal−Organic Framework for Cation Exchange-Based Fe^{3+}-Sensing in an Aqueous Environment. *J. Mater. Chem. A* **2014**, *2*, 13691−13697.